Assessment on BDS-3 PPP/INS Tight Integration by Using Different Orbit/Clock Products

Yu Min [1], Zhouzheng Gao [2] , Jie Lv [3] and Junyao Kan [4]

[1] *School of Land Science and Technology, China University of Geosciences Beijing, Beijing 100083, China*

Abstract

The third-generation BeiDou Navigation Satellite System (BDS-3), which transmits new frequencies, has been completed on June 23rd, 2020. It means that BDS can provide Positioning, Velocimetry, and Timing (PVT) services for global users. However, its performance would be degraded under challenging users' environments. In this paper, we provide the loose and tight integration model between BDS-3 B1I/B2b Precise Point Positioning (PPP) and Inertial Navigation System (INS) to enhance the performance of BDS. Meanwhile, different precise satellite orbit and clock products are used in data processing. Experiment results show that the tight integration model can provide more accurate positioning solutions than that of PPP and PPP/INS loose integration. The impact of orbit/clock products' accuracy on the positioning accuracy is visible. Wherein, the positioning accuracy based on final orbit/clock products presents the best performance with about 3%, 19%, and 19% improvements in the north, east, and vertical components, respectively, compared to that calculated by rapid and ultra-rapid orbit/clock products.

Keywords

Third-generation BeiDou Navigation Satellite System, B1I and B2b, PPP/INS integration

1. Introduction

China decided to build the BeiDou Navigation Satellite System (BDS) at the end of last 20th century. According to the three-step strategy, BDS-1 was completed in 2003. BDS-2 constellation was completed at the end of 2012 with 14 satellites in orbit and BDS-3 was completed on June 23, 2020, with 30 satellites in orbit [1]. Compared to BDS-1 and BDS-2, BDS-3 transmits three new frequencies, namely B1C (1575.42MHz), B2a (1176.45MHz), and B2b (1176.45MHz). Wherein, B2b is a unique frequency for BDS-3, in which both ranging signal and precise satellite orbit/clock corrections are provided. By using the orbit/clock corrections and broadcast ephemeris together, real-time Precise Point Positioning (PPP) can be used.

According to the definition of PPP, it can provide high-accuracy position solutions by using only a single receiver and the precise satellite orbit/clock product [2][3]. Currently, PPP can be divided into ionospheric-free combination PPP (IF PPP) [3], UofC PPP model [4], and Uncombined and Undifferenced PPP model [5][6]. Based on the methods to deal with the ionospheric delay. An Uncombined Undifferenced PPP model based on single/dual/triple frequencies BDS-2/BDS-3 data is introduced in [7]. The results show that the solutions calculated by the BDS-3 new signal present high accuracy in terms of Root Mean Square (RMS) error than that of BDS-2 (B1I+B3I). The accuracy of triple-frequency PPP is close to those of dual-frequency PPP. According to [8], the result indicated that the third frequency will bring improvements when observations on B1I and B2I are contaminated.

However, the performance of PPP would be degraded while suffering challenging environments (such as in the tunnels or under the bridge) [9]. To improve PPP's performance under those conditions,

IPIN 2022 WiP Proceedings, September 5–7, 2022, Beijing, China
EMAIL: mrminyu123@163.com (Yu Min); zhouzhenggao@126.com (Zhouzheng Gao); lvjiecugb@163.com (Jie Lv)
ORCID: 0000-0002-7883-7455 (Yu Min)

usually, the Inertial Navigation System (INS) is utilized to form the PPP/INS integration system. Because INS can autonomically provide continuous position, velocity, and attitude by only processing measurements of the carrier output from Inertial Measurement Units (IMU) without external observations. Such character makes it possible to restrain the drawback of PPP in a poor environment effectively. However, IMU errors will accumulate over time. The integration of PPP and INS can compensate IMU errors online and restrain the divergence [9-11].

The definition of GPS and INS was proposed in 1978 [12]. Last decades, researchers did many works on the integration models of PPP and INS. In [13], a PPP/INS Loosely Coupled Integration (LCI) model is presented, and the results show that INS has a positive impact on PPP accuracy improvement. Own to the fact that LCI mode only can be worked when there are PPP solutions, hence, LCI will stop work under the satellite signal blocked areas where no PPP solutions are obtained. Therefore, a Tightly Coupled Integration (TCI) model is mentioned in [14] to get ideal solutions under satellite-denied environments. According to its conclusions, the horizontal positioning accuracy can be better than 15cm even when the satellite number is less than 4. In [15], PPP/INS TCI system is realized based on a low-cost IMU.

Currently, real-time PPP-related algorithms are becoming the research hotspot. Besides the final products, International GNSS Service (IGS) officially provided ultra-rapid products in November 2011 and established the Real-Time Service (RTS) centers in 2013. Recently, IGS centers such as Wuhan University (WHU) and Centre National d'Etudes Spatiales (CNES) also provide real-time satellite corrections products [16].

Therefore, we provide a tight integration model based on BDS-3 B1I/B2b PPP and low-cost IMU in this paper. Meanwhile, to evaluate the performance of such a model in real-time, a set of vehicle-borne data and the final/rapid/ultra-rapid orbit/clock products are utilized.

2. Methodology

The mathematical models of B1I/B2b PPP, PPP/INS loose integration, and PPP/INS tight integration are described.

2.1. B1I/B2b PPP observational function

Ionosphere-free pseudo-range (P_{IF}) and carrier-phase (L_{IF}) based on B1I and B2b can be described as [9]:

$$P_{IF}=\frac{f_1^2}{f_1^2-f_2^2}P_1-\frac{f_2^2}{f_1^2-f_2^2}P_2=\rho+c\left(t_r-t^s\right)+T_r^s+Re_r^s+Er_r^s+Pco_{r,P_{IF}}^s+Pcv_{r,P_{IF}}^s+Tid_r^s+Gra_r^s+\varepsilon_{P,P_{IF}} \quad (1)$$

$$L_{IF}=\frac{f_1^2}{f_1^2-f_2^2}L_1-\frac{f_2^2}{f_1^2-f_2^2}L_2=\rho+c\left(t_r-t^s\right)+T_r^s-\lambda_{IF}N_{IF}+Re_r^s+Er_r^s+Pco_{r,L_{IF}}^s+Pcv_{r,L_{IF}}^s+Tid_r^s+Gra_r^s+Ph_{r,L_{IF}}^s+\varepsilon_{L,L_{IF}} \quad (2)$$

where r and s represent receiver and satellite; ρ is the geometric range between satellite and receiver; c is the speed of light; t_r and t^s represent the receiver clock offset and satellite clock offset; T_r^s is the tropospheric delay; λ_{IF} is the IF wavelength; N_{IF} is the IF float ambiguity in cycles; $Pcv_{r,L_{IF}}^s$ and $Pcv_{r,P_{IF}}^s$ are the phase center variation project to carrier phase and pseudo-range observation; $Pco_{r,L_{IF}}^s$ and $Pco_{r,P_{IF}}^s$ represent the phase center offset project carrier phase and pseudo-range observation; Tid_r^s is tidal loading; Gra_r^s is gravity error; $Ph_{r,L_{IF}}^s$ is phase windup; Er_r^s represents the earth rotation delay; Re_r^s is the relativistic delay; $\varepsilon_{L,L_{IF}}$ and $\varepsilon_{P,P_{IF}}$ are the measurement noise and unmodeled errors of carrier phase and pseudo-range observation.

2.2. Loosely coupled integration model

The measurement function and state function of loosely coupled integration can be described respectively as [13,16]

$$Z_{LCI,k} = H_{LCI,k} X_{LCI,k} + \eta_{LCI,k}, \eta_{LCI,k} \sim N\left(0, R_{LCI}\right) \tag{3}$$

$$X_{LCI,k} = \phi_{LCI,k,k-1} X_{LCI,k-1} + \mu_{LCI,k-1}, \mu_{LCI,k-1} \sim N\left(0, Q_{LCI,k}\right) \tag{4}$$

where $X_{LCI,k}$ represents the parameter vector; $H_{LCI,k}$ is coefficient matrix; $Z_{LCI,k}$ is the innovation vector; $\eta_{LCI,k}$ represents the vector of observation noise with the prior covariance of R_{LCI}; $\phi_{LCI,k,k-1}$ is the state transition matrix which can be obtained by using the PSI angle model and first-order Gauss-Markov model [13]; $\mu_{LCI,k-1}$ represents the state noise with the prior covariance of $Q_{LCI,k}$.

The innovation vector $Z_{LCI,k}$ can be expressed as

$$Z_{LCI,k} = \begin{bmatrix} C_n^e\left(p_{PPP}^e - p_{INS}^e\right) + C_1 \\ v_{PPP}^n - (v_{INS}^n - \left(\omega_{en}^n \times + \omega_{ie}^n \times\right) C_1 - C_1 \omega_{ib}^b \end{bmatrix} \tag{5}$$

$$C_1 = C_b^n l_b \tag{6}$$

where n, e, b, i are the navigation frame (n), the Earth-Centered Fixed reference frame (e), the body frame (b), and the inertial frame (i); C_n^e (C_b^n) represents the rotation matrix from the n-frame (b-frame) to the e-frame (n-frame); p_{INS}^n and v_{INS}^n are the position and velocity of INS; p_{PPP}^n and v_{PPP}^n represent the position and velocity results of PPP; l^b represents the lever-arm; ω_{ie}^e is the angular rotation rate of e-frame related to i-frame project to e-frame; ω_{ib}^b represents gyro's angular measurements in b-frame; ω_{en}^n is the angular rotation rate of n-frame related to e-frame project to n-frame.

The parameter vector $X_{LCI,k}$ can be described as

$$X_{LCI,k} = \begin{bmatrix} \delta p_{INS}^n & \delta v_{INS}^n & \delta \psi & \delta B_a & \delta B_g & \delta S_a & \delta S_g \end{bmatrix}^T \tag{7}$$

where δp_{INS}^n and δv_{INS}^n represent the position and velocity corrections under n frame; $\delta\psi$ is attitude correction; δS_g and δB_g represent the scale factor and bias of gyroscope; δS_a and δB_a represent the scale factor and bias of accelerometers. The coefficient matrix $H_{LCI,k}$ can be expressed as

$$H_{LCI,k} = \begin{bmatrix} I & 0 & \left(C_b^n l^b \times\right) & 0 & 0 & 0 & 0 \\ 0 & I & H_{v,\psi} & 0 & H_1 & 0 & H_1 \omega_{ib}^b \end{bmatrix} \tag{8}$$

$$H_{v,\psi} = -\left(\omega_{in}^n \times\right)\left(l^b \times\right) - \left(l^b \times \omega_{ib}^b\right) \tag{9}$$

$$H_1 = C_b^n\left(l^b \times\right) \tag{10}$$

Based on the models above, the extended Kalman filter can be used for parameter estimation.

$$\begin{cases} X_{LCI,k,k-1} = \phi_{LCI,k,k-1} X_{LCI,k-1} \\ P_{LCI,k,k-1} = \phi_{LCI,k,k-1} X_{LCI,k-1} \phi_{LCI,k,k-1}^T + Q_{LCI.k-1} \end{cases} \tag{11}$$

$$\begin{cases} X_{LCI,k} = X_{LCI,k,k-1} + K_k\left(Z_{LCI,k} - H_{LCI,k} X_{LCI,k,k-1}\right) \\ P_{LCI,k} = \left(I - K_k H_{LCI,k}\right) P_{LCI,k,k-1}\left(I - K_k H_{LCI,k}\right)^T + K_k R_{LCI} K_k^T \end{cases} \tag{12}$$

where K_k is the Kalman gain matrix.

2.3. Tightly coupled integration model

Different from loose integration, PPP/INS tight integration model uses the raw observation of BDS-3. Similarly, the observation function can be expressed as [10,17]

$$Z_{TCI,k} = H_{TCI,k} X_{TCI,k} + \eta_{TCI,k}, \eta_{TCI,k} \sim N(0, R_{TCI}) \tag{13}$$

with

$$Z_{TCI,k} = \begin{bmatrix} P_{GNSS,PC} - P_{INS,PC} \\ L_{GNSS,LC} - L_{INS,LC} \\ \dot{P}_{GNSS,DC} - \dot{P}_{INS,DC} \end{bmatrix} = \begin{bmatrix} Z_{P_{PC}} \\ Z_{L_{LC}} \\ Z_{\dot{P}_{DC}} \end{bmatrix} \tag{14}$$

$$Z_{P_{PC}} = \alpha P_1 + \beta P_2 - \left\| p_r^e - p_s^e - C_n^e C_b^n l^b \right\| - \Delta P_{PC} + \eta_{P_{pc}} \tag{15}$$

$$Z_{L_{LC}} = \alpha L_1 + \beta L_2 - \left\| p_r^e - p_s^e - C_n^e C_b^n l^b \right\| - \Delta L_{LC} + \eta_{L_{LC}} \tag{16}$$

$$Z_{\dot{P}_{DC}} = \alpha \dot{P}_1 + \beta \dot{P}_2 - \left\| v_r^e - v_s^e - \left[\left(\omega_{in}^n \times \right) C_b^n l^b + C_b^n \left(l^b \times \right) \omega_{ib}^b \right] \right\| - (\Delta \dot{P}_{DC} + \eta_{\dot{P}_{DC}}) \tag{17}$$

where α and β are coefficient of Ionosphere-free combination; $Z_{P_{PC}}$, $Z_{L_{LC}}$, $Z_{\dot{P}_{DC}}$ are the innovation vector of pseudo-range, carrier-phase, and Doppler that are calculated by making a difference operation between BDS-3 measurements ($P_{GNSS,PC}$, $L_{GNSS,LC}$, and $\dot{P}_{GNSS,DC}$) and the corresponding INS predicted values ($P_{INS,PC}$, $L_{INS,LC}$, and $\dot{P}_{INS,DC}$); $\|(\ )\|$ represents modular operation; $\times$ is vector cross product operation, p_s^e and v_s^e are satellite's position and velocity in e-frame; p_r^e and v_r^e represent receiver's position and velocity; ΔP_{PC}, ΔL_{LC} and $\Delta \dot{P}_{DC}$ are sum of pseudo-range errors, carrier-phase errors, and Doppler errors; $\eta_{P_{pc}}$, $\eta_{L_{LC}}$, and $\eta_{\dot{P}_{DC}}$ are observing noise; $\eta_{TCI,k}$ represents the vector of observation noise with the prior covariance of R_{TCI}; other symbols have the same meanings as above.

The parameter vector can be expressed as

$$X_{TCI,k} = \begin{bmatrix} \delta p_{INS}^n & \delta v_{INS}^n & \delta \psi & \delta B_a & \delta B_g & \delta S_a & \delta S_g & \delta t_r & \delta \dot{t}_r & \delta d_{wet} & \delta N_{IF} \end{bmatrix}^T \tag{18}$$

where δt_r and $\delta \dot{t}_r$ are receiver clock offset and receiver clock drift, δd_{wet} is wet component of tropospheric zenith delay and δN_{IF} represents carrier ambiguity.

The coefficient matrix $H_{TCI,k}$ can be obtained by making the differential operation on Eqs. (15), (16), and (17)

$$H_{TCI,k} = \begin{bmatrix} AC_1 & 0 & H_2 & 0 & 0 & 0 & 0 & H_{t_r} & 0 & 0 \\ AC_1 & 0 & H_2 & 0 & 0 & 0 & 0 & H_{t_r} & 0 & I \\ AD^{-1}C_2 & AC_n^e & H_{v,\psi,TCI} & 0 & -AC_n^e H_1 & 0 & H_3 & 0 & H_{\dot{t}_r} & 0 \end{bmatrix} \tag{19}$$

$$H_2 = AC_1 \left(C_b^n l^b \times \right) \tag{20}$$

$$H_3 = -AC_n^e H_1 diag(\omega_{ib}^b) \tag{21}$$

$$H_{v,\psi,TCI} = -AC_n^e \left[(\omega_{en}^n \times + \omega_{ie}^n \times) H_1 + C_b^n (l^b \times \omega_{ib}^b) \times \right] + AD^{-1} C_2 (C_b^n l^b \times) \tag{22}$$

$$D^{-1} = \begin{bmatrix} 1/(R_M + h) & 0 & 0 \\ 0 & 1/(R_N + h)\cos(B) & 0 \\ 0 & 0 & -1 \end{bmatrix} \tag{23}$$

where A represents the direction cosine matrix of satellite-receiver; H_{t_r} and $H_{\dot{t}_r}$ are the coefficient of receiver clock offset and receiver clock drift; C_1 is the transition matrix to transform position corrections from the e-frame to n-frame.

The state equation of TCI can be expressed as

$$X_{TCI,k} = \phi_{TCI,k,k-1} X_{TCI,k-1} + \mu_{TCI,k-1}, \mu_{TCI,k-1} \sim (0, Q_{TCI,k}) \tag{24}$$

where $\phi_{TCI,k,k-1}$ is the system transition matrix from epoch $k-1$ to epoch k; $\mu_{TCI,k-1}$ represent the state noise with the covariance of $Q_{TCI,k}$.

The algorithm structure of TCI and LCI can be shown in Fig. 1.

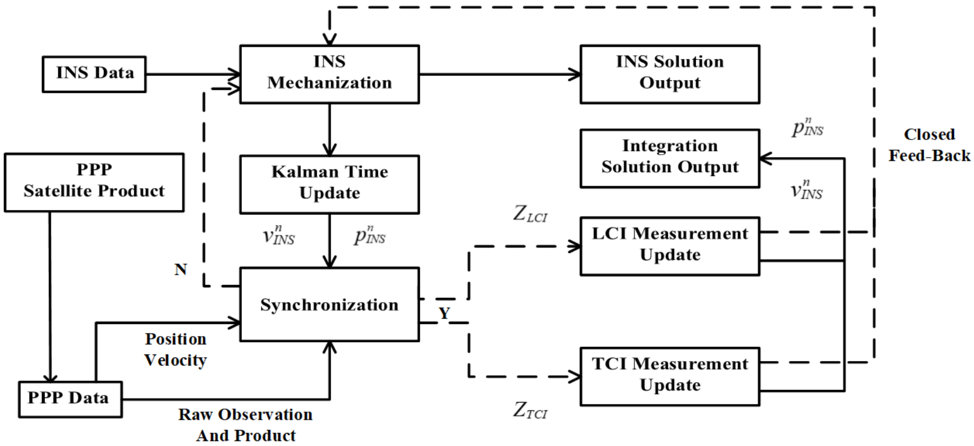

Figure 1: Algorithm structure of PPP/INS loose integration and PPP/INS tight integration

3. Experiment and Results

To evaluate the performance of those positioning methods using BDS-3 final/rapid/ultra-rapid orbit/clock products, a vehicle-borne experiment was arranged in Beijing on December 23, 2021. The equipments are a NovAtel GNSS receiver and a low-cost IMU INS616. The data sampling rate of BDS-3 and IMU are 1HZ and 125HZ. The solutions calculated by Inertial Explorer (IE) software's RTK/INS tight integration are used as reference values. The position differences by making a difference operation between the reference values and the solutions from PPP, PPP/INS LCI, and PPP/INS TCI are transformed into North-East-Up coordinate system. The trajectory of the experiment is shown in Fig. 2. The average number of satellites is 9.24, and the corresponding PDOP value is 2.07 (as shown in Fig. 3). According to Fig. 3, the data before 1300 s are collected almost in open sky conditions, and the observational condition becomes unexpected after 1300 s.

Figure 2: Trajectory of the vehicle-borne test.

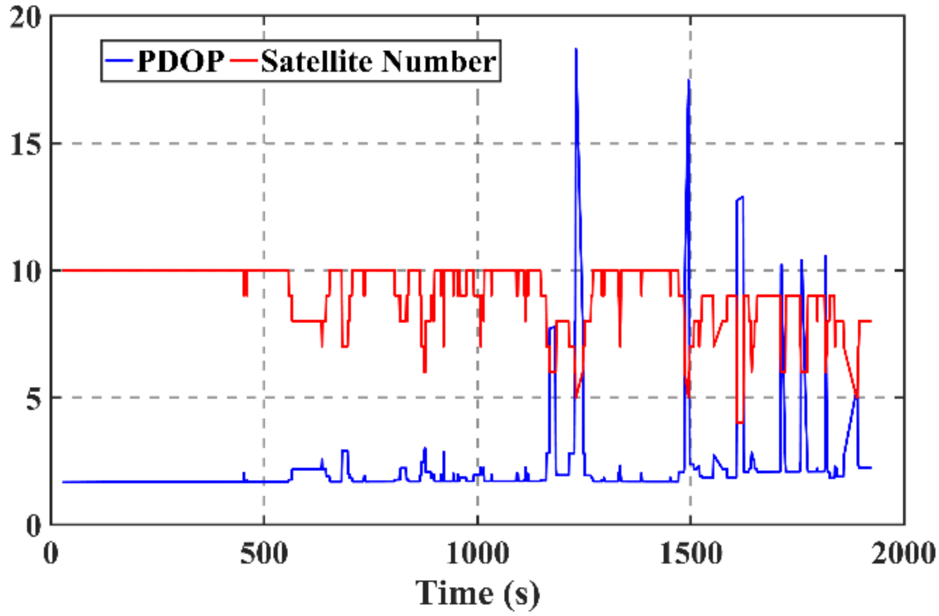

Figure 3: BDS-3 available satellite number and the corresponding PDOP.

Fig. 4 shows the position differences of PPP, PPP/INS LCI, and PPP/INS TCI in the north, east, and vertical directions by using the ultra-rapid precise BDS-3 orbit/clock products. Similar to the trend of the number of satellites, position accuracy before 1300 s performs much better than those after 1300 s. In contrast, PPP/INS TCI mode provides the highest accuracy solutions compared to those of PPP and PPP/INS LCI, especially during the satellites partially blocked environments. The corresponding statistics in terms of RMS are listed in Table 1. Accordingly, the position RMSs of PPP are upgraded from 58.64 cm, 45.15 cm, and 99.47 cm to 38.40 cm, 26.84 cm, and 52.37 cm by PPP/INS TCI with the improvements of 34.52%, 40.55%, and 47.35% in the north, east, and vertical components. Compared to the solutions of TCI with that of LCI, visible improvements in the east and vertical directions (35.79% and 43.55%) can also be found. It may be due to the fact that BDS-3 PPP/INS TCI mode can work even while there are not enough available satellite for PPP calculation. In order to furtherly evaluate the high-accuracy positioning capability of the PPP/INS TCI, the distribution of these position differences calculated by the schemes above are shown in Fig.5. The results show that there are about 0.05%, 0.38%, and 24.06% horizontal position differences within 0.1 m for the PPP, PPP/INS LCI, and PPP/INS TCI, respectively. Such percentages of the horizontal position differences larger than 1.0 m are about 13.22%, 10.16%, and 3.38%. For the vertical component, the percentages of position differences larger than 1.0 m are 17.78% , 17.55%, and 6.78% for PPP, PPP/INS LCI, and PPP/INS TCI, respectively.

Fig.6 shows the position differences of PPP/INS TCI by using the final/rapid/ultra-rapid BDS-3 satellite orbit/clock products. The corresponding statistics are given in Table 2. The position RMS of PPP/INS TCI using final product are 37.20 cm, 21.71 cm, and 42.02 cm with the improvements of 3.1%, 19.11%, and 19.76% in the north, east, and up directions compared with those calculated by using ultra-rapid products. However, the RMS differences between the rapid products-based solutions and those based on ultra-rapid products are invisible. Fig.7 shows the distribution of the position differences of PPP/INS TCI using different orbit/clock products. The results indicate that the percentages of the horizontal position differences within 0.1 m are 4.8%, 15.8% and 24.06% while using the final, rapid and ultra-rapid products in the PPP/INS TCI. Such percentages of the horizontal position differences larger than 1.0 m are 3.33%,3.36%, and 3.38%. For the vertical component, the percentages of position differences larger than 1.0 m are 3.69% , 5.98%, and 5.88% of the three type products.

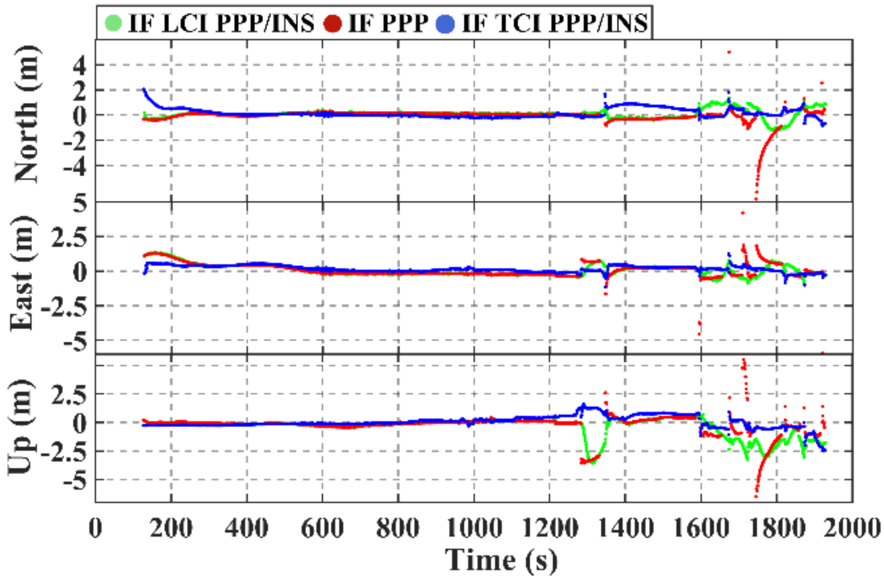

Figure 4: Positioning differences of PPP, PPP/INS LCI, and PPP/INS TCI using ultra-rapid satellite product.

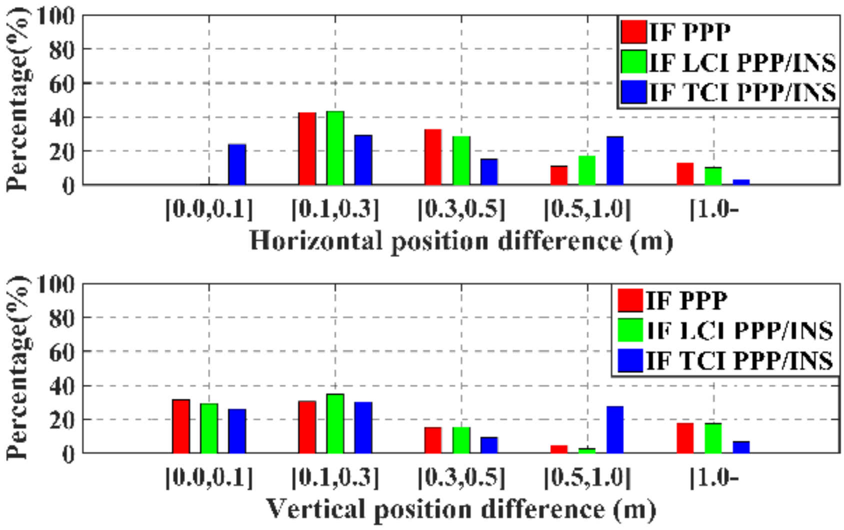

Figure 5: Distribution of the position differences of PPP, PPP/INS LCI, and PPP/INS TCI using ultra-rapid satellite product.

Table 1

Position RMS of different positioning models

Scheme	RMS(cm)		
	North	East	Up
IF PPP	58.64	45.15	99.47
IF LCI PPP/INS	37.05	41.80	92.78
IF TCI PPP/INS	38.40	26.84	52.37

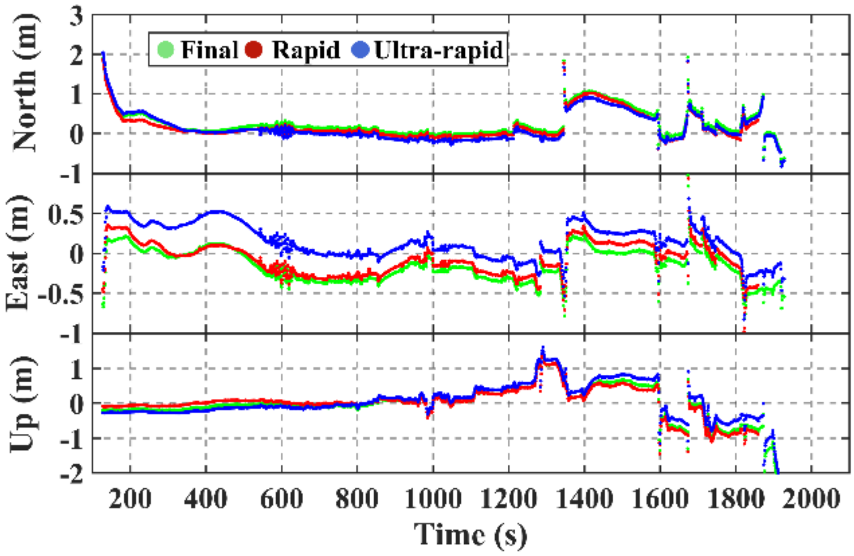

Figure 6: Positioning differences of PPP/INS TCI using different orbit/clock product

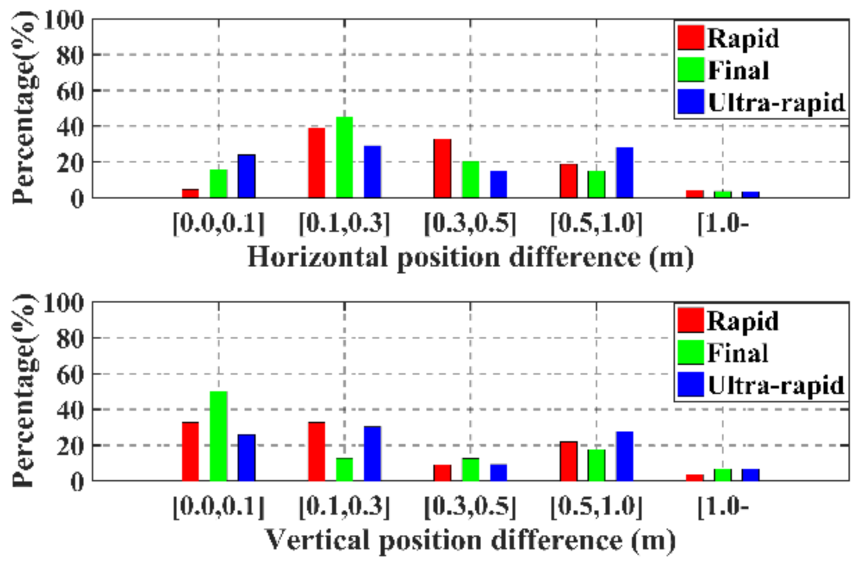

Figure 7: Distribution of the position differences of PPP/INS TCI using different orbit/clock products.

Table 2
Position RMS of PPP/INS TCI by using different product

Product	RMS(cm)		
	North	**East**	**Up**
Final	37.20	21.71	42.02
Rapid	41.69	25.67	53.83
Ultra-rapid	38.40	26.84	52.37

4. Conclusions

This paper evaluates the impacts of different orbit/clock products on the positioning accuracy of the BDS-3 B1I and B2b signal-based PPP/INS tight integration model. The results carried out from vehicle-borne experiment data demonstrate that PPP/INS tight integration can provide more reliable and continuous positioning solutions than PPP and IPPP/INS loose integration, especially while suffering poor BDS observing conditions. Meanwhile, the positioning accuracy of BDS-3 PPP/INS tight integration can provide decimeter-level positioning accuracy by using ultra-rapid products.

5. Acknowledgements

This study is funded by the National Key Research and Development Program of China (Grant No. 2020YFB0505802).

6. Reference

[1] Z. Chen, M. Bai, J. Lei, Y. Huang, J. Wang, and X. Xia, "Comparison of UKF and EKF filter algorithm in INS / BDS tightly mode," Proc. 30th Chinese Control Decis. Conf. CCDC 2018, pp. 2730–2735, 2018.

[2] L. Huang et al., "The performance analysis of multi-system integrated precise point positioning (PPP)," Lect. Notes Electr. Eng., vol. 390, pp. 317–326, 2016.

[3] J. F. Zumberge, M. B. Heflin, D. C. Jefferson, M. M. Watkins, and F. H. Webb, "Precise point positioning for the efficient and robust analysis of GPS data from large networks," J. Geophys. Res. Solid Earth, vol. 102, no. B3, pp. 5005–5017, 1997.

[4] Y. Gao and X. Shen, "A New Method for Carrier-Phase-Based Precise Point Positioning," Navigation, vol. 49, no. 2, pp. 109–116, 2002.

[5] X. Li, M. Ge, H. Zhang, and J. Wickert, "A method for improving uncalibrated phase delay estimation and ambiguity-fixing in real-time precise point positioning," J. Geod., vol. 87, no. 5, pp. 405–416, 2013.

[6] R. Tu, M. Ge, H. Zhang, and G. Huang, "The realization and convergence analysis of combined PPP based on raw observation," Adv. Sp. Res., vol. 52, no. 1, pp. 211–221, 2013.

[7] L. A. Jie et al., "Modeling and assessment of multi-frequency GPS/BDS-2/BDS-3 kinematic precise point positioning based on vehicle-borne data - ScienceDirect," Measurement, vol. 189, 2021.

[8] F. Guo, X. Zhang, J. Wang, and X. Ren, "Modeling and assessment of triple-frequency BDS precise point positioning," J. Geod., vol. 90, no. 11, pp. 1223–1235, 2016.

[9] W. Sun and Y. Yang, "BDS PPP/INS Tight Coupling Method Based on Non-Holonomic Constraint and Zero Velocity Update," IEEE Access, vol. 8, pp. 128866–128876, 2020.

[10] Z. Gao et al., "Tightly coupled integration of multi-GNSS PPP and MEMS inertial measurement unit data," GPS Solut., vol. 21, no. 2, pp. 377–391, 2017.

[11] Z. Gao et al., "Tightly coupled integration of ionosphere-constrained precise point positioning and inertial navigation systems," Sensors (Switzerland), vol. 15, no. 3, pp. 5783–5802, 2015.

[12] D. B. J. Cox, "Integration of GPS with Inertial Navigation Systems," Navigation, vol. 25, no. 2, pp. 236–245, 1978.

[13] A. Q. Le and J. Lorga, "Combining Inertial Navigation System With GPS Precise Point Positioning: Flight Test Results," Proc. Int. Tech. Meet. Satell. Div. Inst. Navig., 2006.

[14] H. Martell, "Tightly Coupled Processing of Precise Point Position (PPP) and INS Data," gpsplusins com, 2009.

[15] S. Du and Y. Gao, "Integration of PPP GPS and Low Cost IMU," 2010 Can. geomatics Conf. Symp. Comm. I, ISPRS, Calgary, Alberta, Canada., pp. 15–18, 2010.

[16] M. Elsheikh, W. Abdelfatah, A. Nourledin, U. Iqbal, and M. Korenberg, "Low-cost real-time PPP/INS integration for automated land vehicles," Sensors (Switzerland), vol. 19, no. 22, pp. 1–21, 2019.

[17] M. Abd Rabbou and A. El-Rabbany, "Tightly coupled integration of GPS precise point positioning and MEMS-based inertial systems," GPS Solut., vol. 19, pp. 601–609, 2014.